Eur. Phys. J. E (2014) **37**: 118
DOI 10.1140/epje/i2014-14118-x

THE EUROPEAN PHYSICAL JOURNAL E

Regular Article

Convection of colloidal suspensions stratified by thermodiffusion and gravity*

B.L. Smorodin[a] and I.N. Cherepanov

Perm State University, Department of Physics of Phase Transitions, 15 Bukirev str., 614990, Perm, Russia

Received 31 July 2014 and Received in final form 21 October 2014
Published online: 25 November 2014 –

Abstract. The convective stability thresholds and nonlinear evolution of convective rolls are numerically investigated in a plane horizontal layer of a colloidal suspension with positive separation ratio in the case of no-slip, impermeable horizontal boundaries. The characteristics of the steady and oscillatory patterns are analyzed under heating and gravity stratification. The standing and traveling waves are found as stable solutions within certain domains of parameters (on the plane of the Rayleigh and the Boltzmann numbers). Complex bifurcation and spatiotemporal properties are caused by the interaction of gravity sedimentation, Soret-induced gradients, and convective mixing of the fluid.

1 Introduction

Convective instability in a horizontal layer of pure liquid appears as a result of the forward bifurcation and evolution of monotonic disturbances. In molecular binary mixtures with negative separation ratio, the heavy component migrates to the hot regions, thereby decreasing the density stratification in the conductive fluid state. The convection onset in this case is associated with the backward Hopf bifurcation and the growth of the oscillatory perturbations. There is a great variety of spatiotemporal states in the binary mixture convection, such as extended standing and traveling waves and the localized states [1–5]. The rich diversity of the patterns is connected with the evolution of the concentration field. Its redistribution, due to convection and thermodiffusion, affects the change of buoyant force acting on a unit volume of the mixture, and hence the velocity of convective flow.

In the last decade great interest has been focused on theoretical [6–10] and experimental [11–14] investigations of colloid binary mixtures and ferrofluids, in particular, (magnetic colloids) [6,8,11]. In colloidal suspensions gravity stratification plays a role of an important additional mechanism of concentration redistribution. The evolution of a concentration field in ferrofluidis is associated with gravitational stratification [7,9,11], thermal diffusion separation [7,9–14] and magnetophoresis [6,8]. However, in the absence of magnetic field, ferrofluids behave as non-magnetic colloidal suspensions. In this case it possible to describe colloids within the model [7,9] taking into account only the thermal diffusion and gravitational mechanisms of stratification. Since the diffusion coefficients are strongly different for molecular and binary colloidal mixtures, the behaviors of convective flows in these media are different. It was shown [9] that gravitational stratification destroys the mirror-glade symmetry of convective regimes inherent in molecular binary mixtures [4]. The linear theory of the convective stability of a colloidal mixture under gravitational stratification and thermal diffusion was developed in [7,9] for monotonic and oscillatory disturbances. The influence of negative separation ratio, sedimentation length, and Prandtl number on the thresholds of oscillatory convection was studied in [9].

The nonlinear evolution of the traveling waves was investigated only in the absence of thermodiffusion when nanoparticles migrate to hot bottom boundary due to gravity segregation [9]. Complex spatiotemporal properties of convective flows caused by the interaction of the gravity-induced concentration gradient, nonlinear advection, and mixing of the fluid with nanoparticles were considered.

The purpose of the present paper is to describe the results of numerical simulations of the convection in a colloidal suspension whose particles have a positive thermal diffusion coefficient. The colloidal suspension fills a horizontal layer heated from below. In this case thermodiffusion and gravity fluxes have opposite directions. In the quiescent state the heavy nanoparticles collect near the upper (cold) or bottom (heated) boundary depending on the relation between the parameters that characterise the thermal diffusion separation and sedimentation of particles

* Contribution to the Topical Issue "Thermal non-equilibrium phenomena in multi-component fluids" edited by Fabrizio Croccolo and Henri Bataller.

[a] e-mail: bsmorodin@yandex.ru

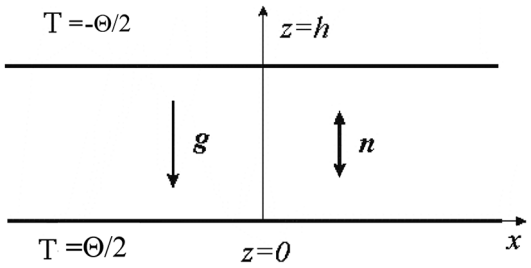

Fig. 1. Problem geometry and coordinate system.

in the gravitational field. In the former case, an unstable stratification of the mixture is formed and convection occurs owing to forward bifurcation. If the heavy nanoparticles collect near the bottom heated boundary, convection occurs owing to backward bifurcation and traveling waves exist in a certain interval of the Rayleigh numbers.

The paper is organized as follows. In sect. 2 we describe the problem formulation, and discuss the mathematical model. Subsection 3.1 contains the linear stability theory of the colloidal suspension quiescent state with respect to small normal perturbations. The computational method and results of direct numerical simulations within the two-dimensional problem are presented in subsect. 3.2. Different convective solutions and the bifurcation maps are discussed in sect. 4.

2 Formulation of the problem

An infinite plane horizontal layer bounded by two parallel rigid plates is filled with a colloidal suspension; its boundaries are impermeable for the mixture components. The x-axis of the Cartesian coordinate system is directed along the layer, while the z-axis is normal to its boundaries (fig. 1). The layer is located in the static gravity field with the acceleration $\boldsymbol{g} = -g\boldsymbol{n}$ ($\boldsymbol{n}$ is an upward unit vector). A vertical temperature gradient is applied to the boundaries: $T(z=0) = \Theta/2$, $T(z=h) = -\Theta/2$. Due to thermal diffusion and gravity sedimentation, a concentration gradient is developed in the mixture.

The equation of state of the mixture can be written in the form

$$\rho = \rho_0(1 - \alpha\delta T + \beta\delta C).$$

Here $\delta T = T - T_*$ and $\delta C = C - C_*$ denote the deviations of the temperature and the concentration of heavier component from their mean values T_* and C_*, respectively; α and β are the thermal and solutal expansion coefficients; ρ_0 is the density of the mixture at the mean values of temperature and concentration.

The governing equations for the velocity v, temperature T and concentration C are the equations of the buoyancy convection within the Oberbeck-Boussinesq approximation [15,16]. Using the layer thickness h for the length, h^2/χ for the time, χ/h for the velocity Θ for the temperature, $\bar{\rho}\nu\chi/h^2$ for the pressure and $C_*h/l_{\rm sed}$ for the concentration ($l_{\rm sed} = k_{\rm B}T_*/(\Delta\rho V g)$ is the sedimentation length, $k_{\rm B}$ is the Boltzmann constant, $\Delta\rho$ is the difference between the densities of the particles and carrier medium, and V is the volume of the particle), one can write the dimensionless equations of the convection colloidal suspension as follows:

$$\begin{aligned}
&\frac{\partial \boldsymbol{v}}{\partial t} + (\boldsymbol{v}\nabla)\boldsymbol{v} = -\nabla p + P\Delta\boldsymbol{v} + P\cdot(RT - BC)\boldsymbol{n},\\
&\frac{\partial T}{\partial t} + (\boldsymbol{v}\nabla)T = \Delta T, \qquad \boldsymbol{n} = (0,0,1),\\
&\frac{\partial C}{\partial t} + (\boldsymbol{v}\nabla)C = L\left[\Delta\left(C + \psi\frac{R}{B}T\right) + \frac{1}{l}\frac{\partial}{\partial z}C\right], \qquad (1)\\
&\qquad \operatorname{div}\boldsymbol{v} = 0,
\end{aligned}$$

where p is the pressure, and the dimensionless parameters $R = g\alpha\Theta h^3/(\nu\chi)$, $B = g\beta C_* h^4/(\nu\chi l_{\rm sed})$, $P = \nu/\chi$, $L = D/\chi$, $l = l_{\rm sed}/h$, $\psi = -\kappa_T\beta_C/(T_*\beta_T) = -C_*(1 - C_*)S_T\beta/\alpha$ are the Rayleigh number, the Boltzmann (or barometric) number [7,9], the Prandtl number, the Lewis number, the dimensionless sedimentation length, and the separation ratio, respectively, while $\kappa_T = T_*C_*(1-C_*)S_T$ is the thermodiffusion coefficient and S_T is the Soret coefficient, ν is the kinematic viscosity, χ is the thermal diffusivity and D is the concentration diffusion constant of the mixture, respectively.

In the equation of concentration we took into account the thermal diffusion effect and the gravity sedimentation of heavy particles. The intensity of the thermal diffusion is characterized by the separation ratio ψ. The sign of this parameter indicates the direction of the mass flux of the solute resulting from the thermal diffusion. We consider the case $\psi > 0$ (the so-called positive Soret coupling), when the heavier component migrates in the direction opposite to the temperature gradient.

The boundary conditions on the horizontal plates are the following:

$$\begin{aligned}
&\boldsymbol{v}(x,0) = \boldsymbol{v}(x,1) = 0,\\
&T(x,0) = 0.5; \quad T(x,1) = -0.5,\\
&\frac{\partial C}{\partial z} + \psi\frac{R}{B}\frac{\partial T}{\partial z} + \frac{1}{l}C = 0 \quad \text{at} \quad z = 0,1. \qquad (2)
\end{aligned}$$

They correspond to no-slip, impermeable for colloidal suspension, and isothermal horizontal plates.

The problem specified by the system of equations (1) and boundary conditions (2) has the conductive distributions of both temperature and nanoparticle concentration in a motionless liquid:

$$\begin{aligned}
&v_0 = 0, \qquad T_0 = 0.5 - z,\\
&C_0 = \frac{e^{-z/l}}{(1 - e^{-1/l})}\left[1 - \frac{\psi R}{B}\right] + \frac{l\psi R}{B}. \qquad (3)
\end{aligned}$$

In the case when

$$R = B/\psi, \qquad (4)$$

the concentration field is homogeneous in the quiescent suspension: $C_0 = l$ in dimensionless form. Using the scales for length and concentration one can see that $C_0 = C_*$.

To solve numerically the problem of convection in the form rolls with axes oriented along the y-axis, stream functions $\Psi(x,z,t)$ and the vorticity $\varphi(x,z,t)$ are introduced:

$$v_x = \frac{\partial \Psi}{\partial z}, \qquad v_z = -\frac{\partial \Psi}{\partial x}, \qquad \varphi = (\mathrm{rot}\, v)_y. \tag{5}$$

Formulation of the problem in terms of the following scalar fields (Ψ, φ, T, C) is written as follows:

$$\begin{aligned}
&\frac{\partial \varphi}{\partial t} + \frac{\partial \Psi}{\partial z}\frac{\partial \varphi}{\partial x} - \frac{\partial \Psi}{\partial x}\frac{\partial \varphi}{\partial z} = P\Delta\varphi - P\cdot\left(R\frac{\partial T}{\partial x} - B\frac{\partial C}{\partial x}\right),\\
&\Delta\Psi = \varphi,\\
&\frac{\partial T}{\partial t} + \frac{\partial \Psi}{\partial z}\frac{\partial T}{\partial x} - \frac{\partial \Psi}{\partial x}\frac{\partial T}{\partial z} = \Delta T,\\
&\frac{\partial C}{\partial t} + \frac{\partial}{\partial x}\left(C\frac{\partial \Psi}{\partial z}\right) - \frac{\partial}{\partial z}\left(C\frac{\partial \Psi}{\partial x}\right) =\\
&\quad L\left(\Delta C + \Psi\frac{R}{B}\Delta T + \frac{1}{l}\frac{\partial}{\partial z}C\right).
\end{aligned} \tag{6}$$

These equations are supplemented with boundary conditions

$$\begin{aligned}
&z = 0: \qquad \Psi = 0, \qquad \frac{\partial \Psi}{\partial z} = 0, \qquad T = 0.5,\\
&\frac{\partial C}{\partial z} + \psi\frac{R}{B}\frac{\partial T}{\partial z} + \frac{1}{l}C = 0,\\
&z = 1: \qquad \Psi = 0, \qquad \frac{\partial \Psi}{\partial z} = 0, \qquad T = -0.5,\\
&\frac{\partial C}{\partial z} + \psi\frac{R}{B}\frac{\partial T}{\partial z} + \frac{1}{l}C = 0,
\end{aligned} \tag{7}$$

The lateral boundary conditions of the computational domain are treated as periodic, therefore all the fields $\mathcal{F} \equiv \{\Psi, \varphi, T, C\}$ in x-direction are set to periodic

$$\mathcal{F}(x,z,t) = \mathcal{F}(x+\lambda, z, t). \tag{8}$$

In the present paper, we employ the set of parameters that is typical of colloidal suspension: the Lewis number $L = 10^{-4}$, the Prandtl number $P = 10$, and separation ratio $\psi > 0$.

3 Numerical results

3.1 Linear stability analysis

First, we briefly discuss the behaviour of small disturbances of the basic state (2). let us consider small normal disturbances of the conductive state (2) taken as

$$\{\Psi, \tilde{T}, \tilde{c}\} = \exp(\gamma t + ikx)\{\Psi(t,z), \theta(t,z), \xi(t,z)\}, \tag{9}$$

here γ is the growth rate of the disturbances, $k = 2\pi/\lambda$ is the wave number.

After linearization one can obtain the following spectral boundary value problem for small normal disturbances:

$$\begin{aligned}
&\gamma\left(\frac{\mathrm{d}^2}{\mathrm{d}z^2} - k^2\right)w = P\left(\frac{\mathrm{d}^2}{\mathrm{d}z^2} - k^2\right)^2 w - Pk^2(R\theta - B\xi),\\
&\gamma\theta = -w\frac{\partial T_0}{\partial z} + \Delta\theta,\\
&\gamma\xi = -w\frac{\partial C_0}{\partial z} + L\left(\left(\frac{\mathrm{d}^2}{\mathrm{d}z^2} - k^2\right)\left(\xi + \frac{\psi R}{B}\theta\right) + \frac{1}{l}\frac{\partial \xi}{\partial z}\right),
\end{aligned} \tag{10}$$

$$\begin{aligned}
&z = 0, 1: \qquad w = 0, \qquad \frac{\partial w}{\partial z} = 0, \qquad \theta = 0,\\
&\frac{\partial \xi}{\partial z} + \psi\frac{R}{B}\frac{\partial \theta}{\partial z} + \frac{1}{l}\theta = 0,
\end{aligned} \tag{11}$$

where we use the ratio between vertical velocity and stream function $v_z = w = -ik\Psi$.

We perform the linear stability analysis of the basic state (3) by solving the spectral-amplitude problem (10)-(11). The numerical procedure is based on the shooting (sequential) method with the orthogonalization scheme for integration [17].

The neutral curves of the instability, $R(k)$, are shown in fig. 2 for several values of the Boltzmann number B and $\psi = 10$. The instability domains are located above the curves. The long-wave limit of the instability boundary is determined by relation $R = (B + 720L)/\psi$ [9]. At the small values of Boltzmann numbers only the monotonous instability exists (fig. 2a). The calculation shows that the critical Rayleigh numbers for monotonous disturbances are slightly smaller than the values which are predicted by simple Galerkin approximation $R_c = B/\psi$ [7, 9] (fig. 2). The oscillatory instability appears at some values of the Boltzmann number $B_1(\psi)$. The neutral curves consist of two parts (fig. 2b,c), which reflects the competition between monotonous and oscillatory disturbances with different wavelength. The instability connects with monotonous disturbances in the interval $B_1 < B < B_2$ (fig. 2b) and with the oscillatory ones when $B > B_2$ (fig. 2c). In the case $\psi = 10$ we have $B_1 = 6995$ and $B_2 = 9907$.

The appearance of the oscillatory instability is easily explained with the help of the decrement spectra $\gamma(R)$. Figure 3 shows the behavior of $\gamma_r = \Re(\gamma)$ for some lower levels of the decrement spectra in dependence on the Rayleigh number close to instability boundary. One can see that instability connects with the complex conjugated pair whose real part (blue thick line) crosses the zero level. The imaginary part of this decrement is frequency of the neutral oscillation $\omega = \gamma_i = \Im(\gamma)$. Slightly above the instability boundary the complex conjugated pair transforms into two real levels of the decrement spectra.

In fig. 4 the dependencies of the critical Rayleigh number for monotonous (solid lines) and oscillatory (dashed lines) disturbances are presented *versus* the Boltzmann number at different values of the separation ratio ψ. The growth of value of thermodiffusion parameter corresponding to the greater accumulation of the heavier component

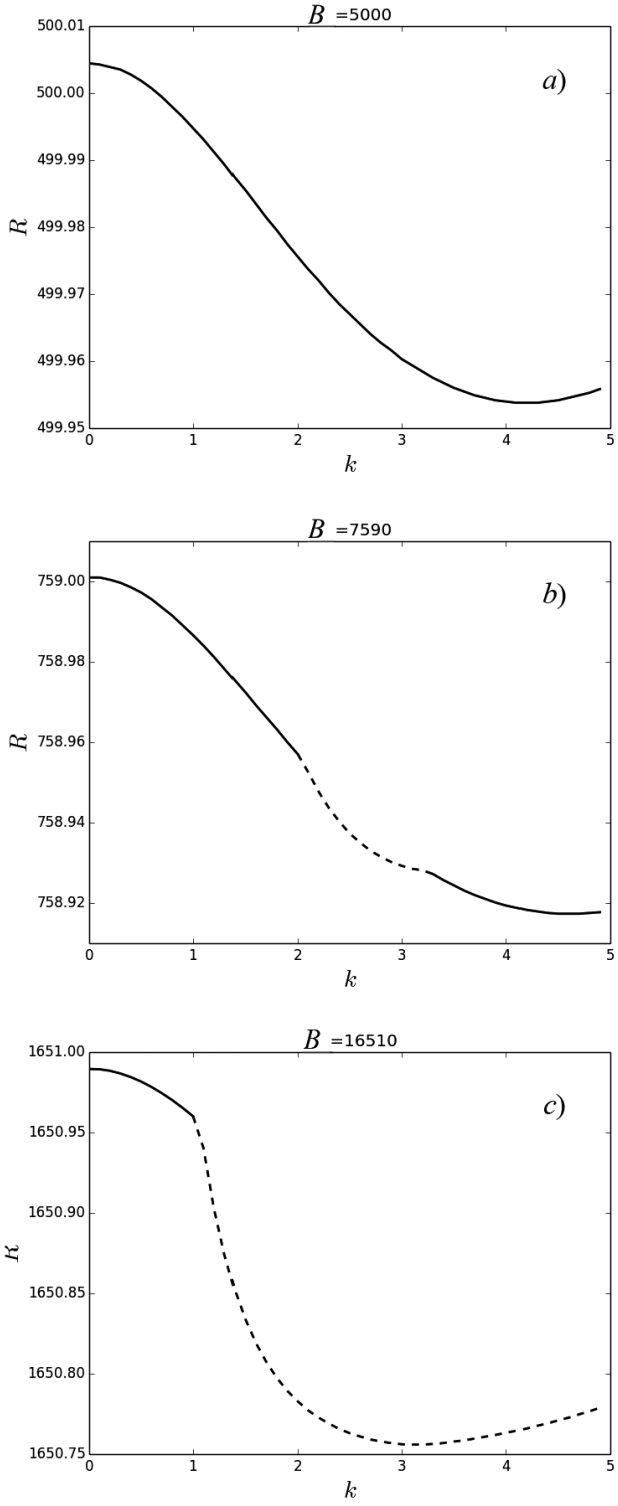

Fig. 2. Neutral stability curves for convection of the colloidal suspension $R\,(k)$ for different Boltzmann number: a) $B = 5000$; b) $B = 7590$; c) $B = 16510$. The other parameters are $\psi = 10$, $L = 10^{-4}$, $P = 10$, $l = 30$.

near the upper cold plate causes the stability boundary to shift down. The increase in the Boltzmann number B corresponding to a stronger gravity stratification stabilizes the quiescent state; the instability boundary increases in

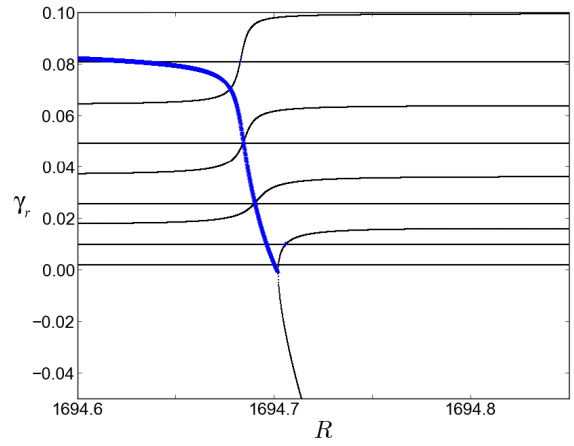

Fig. 3. (Color online) The decrement spectra in dependence on the Rayleigh number R The blue thick lines represent the real part of the complex conjugate decrement pair for oscillation disturbances, thin (black) lines represent real decrements for monotonic disturbances. The parameters are $k = 3.14$, $L = 10^{-4}$, $P = 10$, $l = 30$, $B = 16950$.

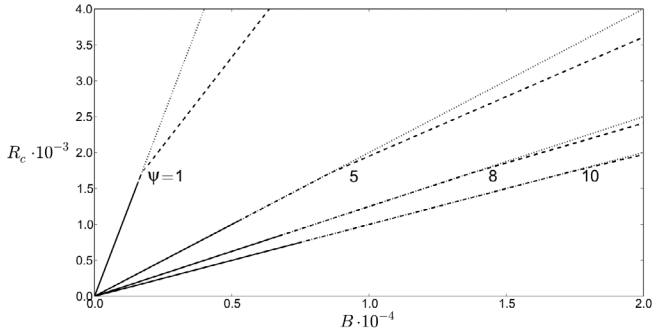

Fig. 4. Critical values of the Rayleigh number $R_{\rm c}$ for monotonous (solid lines) and oscillatory disturbances $R_{\rm osc}(B)$ (dashed lines) *versus* the Boltzmann number B for different values of separation ratio $\psi = 1, 2, 5, 10$. The dotted lines correspond to the law $R = B/\psi$. The other parameters are $L = 10^{-4}$, $P = 10$, $l = 30$.

accordance with the approximate law $R_{\rm c} \approx B/\psi$, which, however, is observed with a good accuracy. In the case $R_{\rm c} > R^0_{\rm st}$ ($R^0_{\rm st}$ is the critical Rayleigh number in a homogeneous fluid) the oscillatory instability $R_{\rm osc}(B)$ comes at lower values of the Rayleigh number than it is predicted by linear law $R_{\rm osc} < B/\psi$.

3.2 The nonlinear evolution of convective patterns

To obtain approximate solutions of the boundary value problem (6)–(8) the finite-difference technique is applied to a set of discrete points, uniformly spaced within the computational domain with respect to each independent variable. In this case, the spatial derivatives of the equations of motion and heat transfer are approximated by central differences. The finite-difference approximation of the equation for the concentration in eqs. (6) should satisfy the mass conservation law. This property is ensured

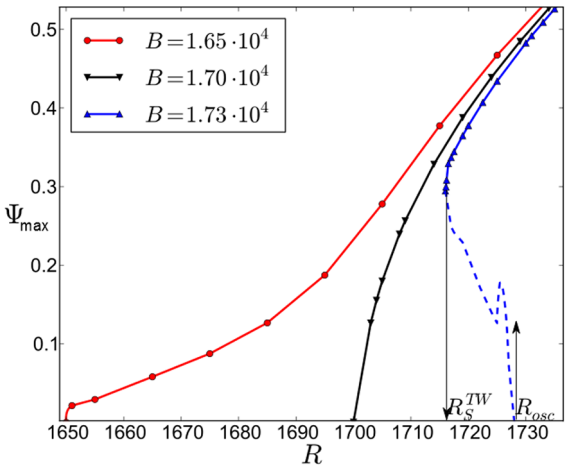

Fig. 5. (Color online) Bifurcation diagram of laterally extended convective states with the wave number $k = \pi$ in the colloidal suspension layer, the maximal values of the stream function as functions of the Rayleigh number R, at $\psi = 10$, $L = 10^{-4}$, $P = 10$, $l = 30$. Solid (or dashed) lines correspond to stable (or unstable) regimes.

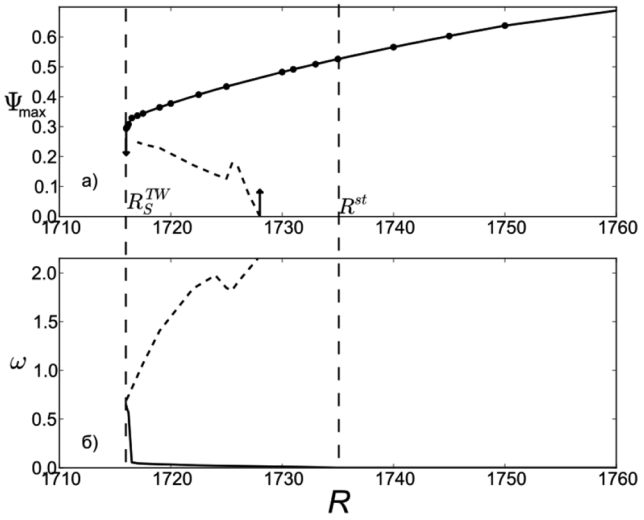

Fig. 6. Bifurcation diagram of laterally extended convective states with the wave number $k = \pi$ in a colloidal suspension as functions of Rayleigh number R. Thin lines refer to the maximal stream function (upper frame) and the frequency (lower frame), with full (dashed) lines denoting stable (unstable) solutions. $B = 1.73 \cdot 10^4$, $\psi = 10$, $L = 10^{-4}$, $P = 10$, $l = 30$.

by the conservative form of the equation and its approximation by the control volume method [18]. The Poisson equation was solved by the successive upper relaxation method. The solution was constructed on a 82×41 grid. The test calculations were performed on a 122×61 grid. Refining the mesh did not have any significant effect on characteristics of the convective regimes.

We monitor the time evolution of the maximum of the stream function Ψ field in the x-z cross section perpendicular to the roll axes

$$\Psi_{\max}(t) = \max_{x,z}[\Psi(x_i, z_j, t_k)], \tag{12}$$

as well as the local time evolution of Ψ at a fixed position $(x = L/4,\ z = 1/2)$

$$\Psi_{\rm loc}(t) = \Psi(x = 4/3, z = 1/2, t). \tag{13}$$

Our numerical code gives the critical Rayleigh number, $R^0_{\rm st} = 1700$, for the onset of convection in a homogeneous liquid.

We are concerned with the properties of the convective system at different values of the Boltzmann number B. The bifurcation diagrams are presented in fig. 5 at three different ratios between thermodiffusion and gravity separation. Let us first consider rather small B values $B = 1.65 \cdot 10^4$ ($B < R^0_{\rm st} \cdot \psi$): the thermodiffusion separation is stronger then gravity sedimentation. In a quiescent liquid the heavy component migrates to upper (cold) boundary. In this case the bifurcation diagram looks like the one for the absence of gravity sedimentation and positive separation ration. When the heating intensity increases quasi-statically, the onset of convection occurs *via* a forward bifurcation at the Rayleigh number value $R_{\rm c}(B)$. The maximum of the stream function Ψ in the convective regime monotonically grows with the increase

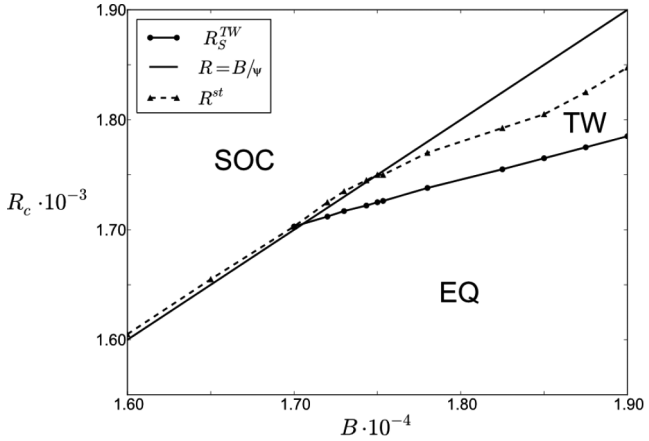

Fig. 7. Map of the regimes on the plane of parameters $\{B, R\}$: mechanical equilibrium (quiescent liquid) EQ, traveling wave TW, steady overturning convection SOC. Critical numbers (line 1) $R_{\rm st}$ and (line 2) $R_{\rm S}^{\rm TW}$ *versus* B for $L = 10^{-4}$, $P = 10$, $\psi = 10$, and $l = 30$. The solid straight line is $R = B/\psi$.

of the Rayleigh number R. The second case, $B = R^0_{\rm st} \cdot \psi$, corresponds to homogeneous liquid: the thermodiffusion flux of heavy colloidal particles to cold upper boundary is compensated by gravity segregation of these particles. In this case one can see the bifurcation diagram of a single component (pure) fluid. If gravity segregation dominates $B > R^0_{\rm st} \cdot \psi$, the onset of convection corresponds to the backward Hopf bifurcation. The dependencies of maximal value of the stream function and oscillation frequency on the Rayleigh number are presented in fig. 6. The two-dimensional right and left traveling wave solutions bifurcate backward out of the conductive state at $R_{\rm osc}(B)$, which is in good agreement with the predictions

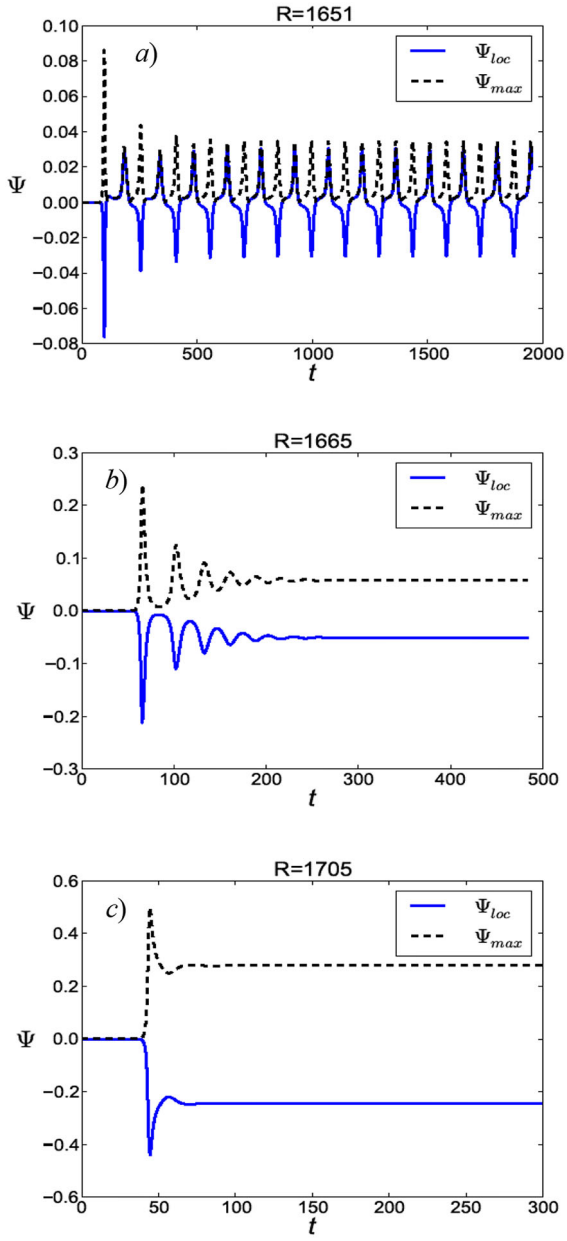

Fig. 8. (Color online) The temporal evolution $\Psi_{\rm loc} = \Psi(x = 4/3,\ z = 1/2, t)$ and $\Psi_{\rm max}$: a) standing wave regime SW at $R = 1651$; b) the transient regime to SOC at $R = 1665$; c) the transient regime to SOC at $R = 1705$; $B = 1.65 \cdot 10^4$, $\psi = 10$, $L = 10^{-4}$, $P = 10$, $l = 30$.

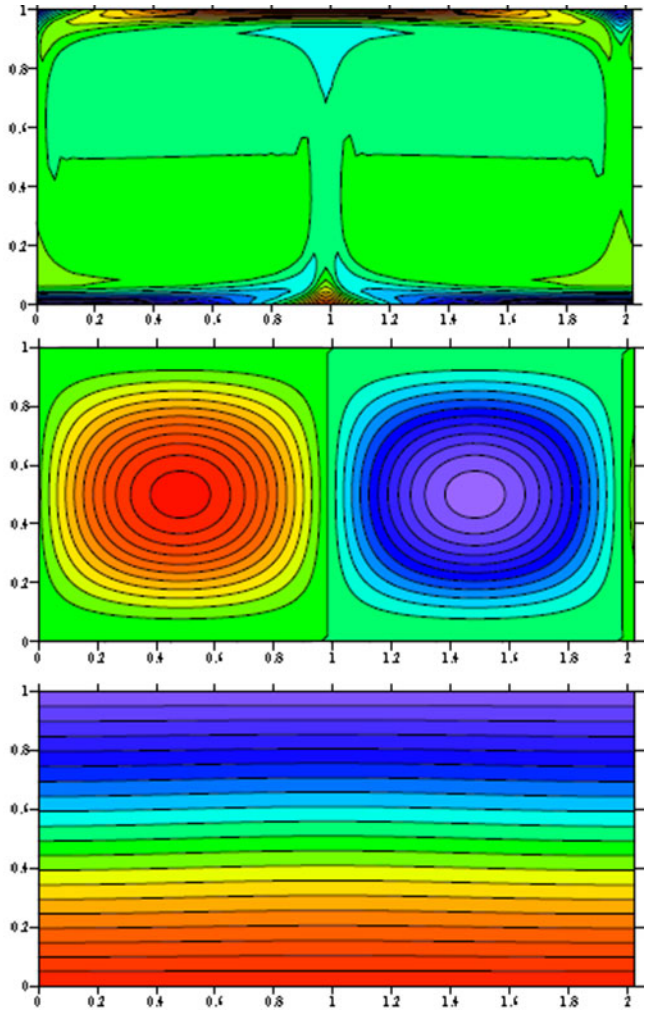

Fig. 9. (Color online) Snapshots of the concentration, stream functions and temperature fields in the convective cell at SOC regime: $R = 1665$; $B = 1.65 \cdot 10^4$, $\psi = 10$, $L = 10^{-4}$, $P = 10$, $l = 30$.

of the linear stability theory (see sect. 3.1). The waves gain stability via a saddle-node bifurcation at the value of Rayleigh number $R_{\rm S}^{\rm TW}(B)$. For instance, at the Boltzmann number $B = 1.73 \cdot 10^4$ the critical Rayleigh number is $R_{\rm osc}(B = 1.73 \cdot 10^4) = 1728$ and the Hopf frequency is $\omega_{\rm H} = 2.23$, the saddle-node point is characterised by the following parameters $R_{\rm S}^{\rm TW}(B = 1.73 \cdot 10^4) = 1716$, $\omega_{\rm S}^{\rm TW} = 0.4$.

Within the interval $R_{\rm S}^{\rm TW} < R < R_{\rm osc}$ both the stable TW regime (solid lines in figs. 5, 6) and the unstable one (dashed lines) exist. As in the case of molecular binary mixture [5], the concentration field is strongly nonlinear in the stable regime, while it is weakly nonlinear when the traveling wave is unstable. Moreover, the S-shape form of the unstable TW branch (fig. 6) connects with the coincidence of the maximal value of the vertical convective velocity $|w| = k\Psi_{\rm max}$ and the phase velocity of the travelling wave $v_{\rm ph} = \omega/k$ [5].

Within the range $R < R_{\rm S}^{\rm TW}$ the binary mixture convection decays and the system relaxes to the conductive state. The branch of stable TWs ends at the value of reduced Rayleigh number $R_{\rm st}(B = 1.73 \cdot 10^4) = 1735$ and the stationary overturning convection (SOC) solution is formed. Thus, the highly developed, nonlinear traveling wave convection is stable within the interval of the reduced Rayleigh numbers $R_{\rm S}^{\rm TW} < R < R_{\rm st}$.

Figure 7 represents the stability diagram of the convection modes in the parameter plane $\{R, B\}$. The steady convection solutions (SOC) are observed at $B < 17000$ above the dashed line. The critical Rayleigh number R

depends linearly on B as $R = B/\psi$. This result is in agreement with the results of linear theory [7,9]. At $B > 17000$, oscillatory perturbations grow and the traveling wave TW regime exists in the range $R_{\rm S}^{\rm TW} < R < R_{\rm st}$. It is shown that the growth of Boltzmann number leads to an increase in the characteristic values of the critical parameter $R_{\rm st}$.

The new oscillating solution in the form of standing wave SW is found slightly above the convective instability boundary when thermodiffusion separation exceeds gravity segregation $B < R_{\rm st}^0 \cdot \psi$. This solution exists in the narrow interval of the Rayleigh number: $\Delta R < 1665 - 1650 = 15$ (fig. 8). The oscillatory instability produces undamped supercritical oscillations which are so weak that they do not destroy the concentration profile completely (fig. 8a). The growth of the Rayleigh number leads to the changing of concentration field and the damping of SW oscillation (fig. 8b,c). The standing wave SW solution transforms into the SOC regime. The stream function, temperature and concentration fields for stationary convective solution are shown in fig. 9 by snapshots in the x-z plane. All fields demonstrate a mirror symmetry between oppositely turning vortices. The convective mixing in SW solution has low intensity so temperature isolines are slightly curved.

4 Conclusion

The influence of gravity sedimentation and thermodiffusion separation on the convective instability and pattern formation in a colloidal suspension is investigated in a horizontal layer heated from below. Finite-difference numerical simulations were carried out for typical of colloidal suspension parameters with positive Soret coupling.

It is shown that an increase of the Boltzmann number leads to an increase of the critical control parameters: Rayleigh numbers $R_{\rm S}^{\rm TW}$, $R_{\rm osc}$, $R_{\rm st}$. The nonlinear convective patterns are found depending on the Rayleigh and Boltzmann numbers: standing wave SW, TW and SOC state. The contour plots of the stream function and concentration fields represent the specific features of SW convective solution. Our results are summarized in bifurcation diagrams displaying the scenarios of possible transitions, as well as the stability map where the observed convection flow patterns are shown.

This work was partially supported by grant provided by the Russian Foundation for Basic Research (projects Nos. 14-01-96027, 14-01-31299).

References

1. E. Moses, J. Fineberg, V. Steinberg, Phys. Rev. A **35**, R2757 (1987).
2. J.J. Niemela, G. Ahlers, D.S. Cannell, Phys. Rev. Lett. **64**, 1365 (1990).
3. D. Bensimon, P. Kolodner, C.M. Surko, H. Williams, V. Croquette, J. Fluid Mech. **217**, 441 (1990).
4. M. Lücke, M.W. Barten, P. Büchel, C. Fütterer, Lect. Notes Phys. **55**, 127 (1998).
5. D. Jung, P. Matura, M. Lücke, Eur. Phys. J. E **15**, 293 (2004).
6. M.I. Shliomis, B.L. Smorodin, S. Kamiyama, Philos. Mag. **83**, 2139 (2003).
7. M.I. Shliomis, B.L. Smorodin, Phys. Rev. E **71**, 036312 (2005).
8. A. Ryskin, H. Pleiner, Phys. Rev. E **75**, 056303 (2007).
9. B.L. Smorodin, I.N. Cherepanov, B.I. Myznikova, M.I. Shliomis, Phys. Rev. E **84**, 026305 (2011).
10. L. Hadji, M. Darassi, Phys. Rev. E **89**, 013014 (2014).
11. T. Tynjälä, A. Bozhko, P. Bulychev, G. Putin, P. Sarkomaa, J. Magn. & Magn. Mater. **300**, 195 (2006).
12. G. Donzelli, R. Cerbino, A. Vailati, Phys. Rev. Lett. **102**, 104503 (2009).
13. M. Bernardin, F. Comitani, A. Vailati, Phys. Rev. E **85**, 066321 (2012).
14. B.H. Chang, A.F. Mills, E. Hernandez, Int. J. Heat Mass Transfer **51**, 1332 (2008).
15. J.K. Platten, J.C. Legros, *Convection in Liquids* (Springer-Verlag, Berlin, Heidelberg, 1984).
16. L.D. Landau, E.M. Lifschitz, *Course of Theoretical Physics*, Vol. **6** (Pergamon Press, Oxford, 1993).
17. U.M. Ascher, R.M.M. Mattheij, R.D. Russell, in *Numerical Solution of Boundary Value Problems for Ordinary Differential Equations, Prentice Hall Series in Computational Mathematics* (Prentice-Hall, Englewood Cliffs, NJ, 1988).
18. P. Roache, *Computational Fluid Dynamics* (Hermosa, Albuquerque, New Mexico, 1976).